Sonic crystal with open resonant cavities

Zhilin Hou
Department of Physics, South China University of Technology, Guangzhou 510640, China and Laboratoire de Physique des Milieux Ionisés et Applications (LPMIA), Université Henri Poincaré, Nancy I Boulevard des Aiguillettes, Boîte Postale 239 F-54506 Vandoeuvre-lès-Nancy, France

Jingtao Liu, Weimin Kuang, and Youyan Liu
Department of Physics, South China University of Technology, Guangzhou 510640, China

Shuizhu Wu*
Department of Polymer Science & Engineering, South China University of Technology, Guangzhou 510640, China
(Received 18 September 2006; published 12 February 2007)

An improved scattering matrix method is developed to study a two-dimensional air-rigid sonic crystal with open resonant cavity, and the band structure and transmission properties are investigated. Numerical results show that both the band structure and the transmission coefficient are sensitive to the shape of the resonant cavity. The relationship between the resonant band gap and the shape of the resonant cavity is given. The high effective refractive index and the transmission ratio in the long wave range make such a system a good material for a sound lens.

DOI: 10.1103/PhysRevE.75.026608 PACS number(s): 43.20.+g, 43.40.+s, 46.40.Cd

I. INTRODUCTION

The so-called sonic crystal (SC) has received much attention in the last decade because of its interesting acoustic wave properties. Compared with the conventional phononic crystals (PCs) which are made of solid or liquid elastic materials, a SC is constructed by solid elastic materials (usually being considered as rigid) and air [1–3]. The spacial structure of SCs can be realized easily in experiment and should have many potential applications. For example, the existence of the absolute frequency band gap(s) (ABGs) [1–6] of SC makes it a good candidate for audible sound proofing. Cervera *et al.* proved that SCs can also be used to make a sound lens to focus sound waves [7]. Recently, Feng *et al.* even proved that the negative refractions can be realized in this kind of system [8].

There are several numerical methods to study PCs, including the plane wave expansion (PWE) method [1–3], the multiscattering theory (MST) [4,9–12], and the finite difference time domain (FDTD) method [5,13,14]. In principle, all of them can be used to deal with SCs, but there are advantages and disadvantages to each method. In the PWE method, the convergence problem and the singularity in the solid/fluid system [15] still exist in SCs. Due to the huge mismatch of the sound impedance between air and solid in SCs, the solid component is usually regarded as a hard and heavy fluid, where only the longitudinal wave can be excited. We have pointed out in Ref. [15] that this hypothesis is physically unacceptable although the results from it are correct. The MST method is very popular in the SC research. But it is argued in Ref. [16] that this method can only be used in systems with a smooth interface between different components, and it will not be applicable to systems consisting of scatterers with a complicated shape. Compared with MST, the FDTD method is more versatile. It can be used to study sophisticated systems to get the band structure and the transmission properties as well. The shortcoming of the FDTD method is that it costs a lot of CPU time.

Using the PWE method, Vasseur *et al.* investigated the sound property of the systems with hollow rigid scatterers for the first time [3]. In this kind of system, the cavity in scatterers does not give any influence to the band structure because of the rigidity of the scatterer's shell. More recently, Sainidou *et al.* studied a similar system [17] in which hollow polymer cylinders and spheres are used as scatterers instead of rigid materials. They observed some dispersiveness bands in the bad gap which are caused by the localized resonant states in hollow scatterers. Hu *et al.* [14] studied a system with one-end-closed resonant cavity by use of the FDTD method. They analyzed the band structure and the transmission property and showed that the resonant modes in cavities can reduce the effective velocity and acoustic impedance of the system. So they suggested that such a composite would be a good material for a sound lens; but they did not give the relationship between the band structure and the size of the cavity in detail.

Recently, we developed a new method named *eigenmode matching theory* (EMMT) to study the solid-solid PCs [16], and later we improved it to deal with the SCs [15], in which the scattering matrix technique is employed. By the improved EMMT method, we successfully solved the problems in the PWE method and we can also treat systems with various shaped scatterers. Furthermore, the band structure and transmission property can be calculated simultaneously. In the present paper, we will further improve this method to study a more complicated SC, which is constructed by rigid scatterers with open resonant cavity and air. As we will see in Sec. II the existence of resonant cavity will make the computation more difficult because the effect of the cavity is included in the scattering matrix [15] and some algebra de-

*Email address: shzhwu@scut.edu.cn

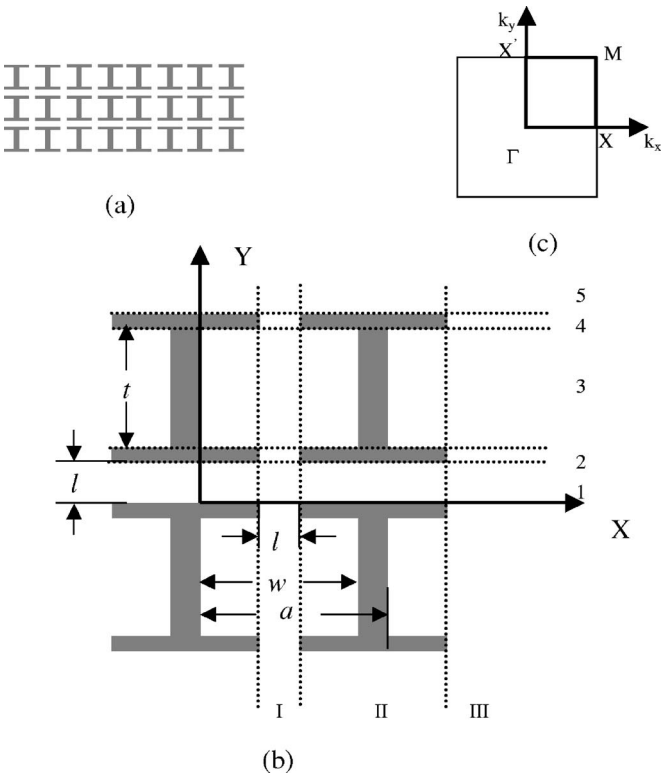

FIG. 1. (a) Bird's-eye view of a two-dimensional sonic crystal constructed by rectangular rods (shaded areas) with an open resonant cavity arranged squarely in a uniform host. (b) The enlarged unit cell of (a), in which a is the lattice constant, w and t are the width and length of the open resonant cavity, and l is the distance between two nearest rods. A set of planes parallel to the yoz (xoz) plane cuts the unit cell into uniform and composite layers along the x (y) direction, which are labeled as $1,2,3,4(I,II)$, respectively. (c) The first Brillouin zone of the considered system.

ductions have to be done. We investigate the relationship between the band structure and the shape of the cavity and find that the band structure of such a system can be strongly adjusted by the shape of the cavity. The introduced cavity not only changes the width of the absolute band gap and its midfrequency, but also changes the low frequency behaviors (usually described by effective velocity and sound impedance). We also find that the PWE method cannot deal with such a system even if the rigid scatterers are considered as fluid with high acoustic impedance.

This paper is organized as follows. We present the main idea and the formulation of the improved EMMT method in Sec. II. The numerical results are shown and the discussions are given in Sec. III. And finally Sec. IV is a brief summary.

II. THE CALCULATION METHOD

We study the two-dimensional (2D) system shown in Fig. 1(a), and the detailed parameters are given in Fig. 1(b). The resonant cavity has width w and length t with an open mouth of width l. Obviously, the structure will reduce to a conventional 2D structure with rectangular rods embedded into air if we set $t=0$ or $w=l$. Figure 1(c) gives the reduced surface Brillouin zone (BZ) of the corresponding structure. For the system with $t=0$ or $w=l$, we can use the method given in Ref. [15], in which the system can be cut into two different layers along the y direction and only one kind of connection condition between different layers needs to be considered. However, for systems with $t\neq 0$ and $w\neq l$, there are several different kinds of layers and connection conditions. Furthermore, the direction ΓX is not equivalent to $\Gamma X'$ because of the anisotropy of the structure. Therefore the calculation methods in directions ΓX and $\Gamma X'$ will be presented separately in the following sections.

A. Along the $\Gamma X'$ direction

As it is shown in Fig. 1(b), the unit cell of the structure can be cut into four different kinds of layers along the y direction. The layer labeled by 1 is the uniform one and the rest of the layers labeled by 2, 3, and 4 are stacked periodically by air and rigid piece. We notice that layers 2 and 4 are identical, but layer 3 has different thickness of the air piece. Following Ref. [15], we can write the wave solution in the uniform layers as a superposition of plane wave modes

$$p(x,y)=\sum_{n=-M}^{+M} e^{i(K_x+G_n)x}[A_n^+e^{i\beta_n y}+A_n^-e^{-i\beta_n y}] \tag{1}$$

and

$$v_y(x,y)=\sum_{n=-M}^{+M}\frac{\beta_n}{\rho\omega}e^{i(K_x+G_n)x}[A_n^+e^{i\beta_n y}-A_n^-e^{-i\beta_n y}], \tag{2}$$

where $p(x,y)$ is the pressure field, $v_y(x,y)$ is the velocity field component along the y direction, ω is the angular frequency of the wave, ρ is the mass density, c is the wave velocity in air, K_x is the Bloch wave vector along the x direction, and A_n^+ (A_n^-) is the amplitude of the positive (negative) propagating waves along the y direction, respectively. G_n is the reciprocal lattice vector and β_n is the wave number along the y direction, which take the values

$$G_n=2n\pi/a \quad (n=0,\pm 1,\ldots,\pm M) \tag{3}$$

and

$$\beta_n=\sqrt{(\omega/c)^2-(K_x+G_n)^2}. \tag{4}$$

The wave solution in the composite layers can be expressed as a superposition of the waveguide modes because waves are confined in the air piece. The pressure and velocity field along the y direction can be expressed as

$$p(x,y)=\sum_{n=0}^{N}\cos\frac{n\pi(x-x_0)}{\lambda}[A_n^+e^{i\beta_n y}+A_n^-e^{-i\beta_n y}] \tag{5}$$

and

$$v_y(x,y)=\sum_{n=0}^{N}\frac{\beta_n}{\rho\omega}\cos\frac{n\pi(x-x_0)}{\lambda}[A_n^+e^{i\beta_n y}-A_n^-e^{-i\beta_n y}], \tag{6}$$

with

$$\beta_n = \sqrt{\left(\frac{\omega}{c}\right)^2 - \left(\frac{n\pi}{\lambda}\right)^2} \quad (n = 0,1,\ldots,N) \tag{7}$$

being the wave vector along the y direction in the air piece. The parameter λ takes different values for different layers, with $\lambda = l$ for layers 2 and 4, and $\lambda = w$ for layer 3. In Eqs. (5) and (6), x_0 is the position shift of the waveguide from the coordinate origin. In the coordinate system chosen as in Fig. 1(b), we have $x_0 = 0$ for layer 3 and $x_0 = (w-l)/2$ for layers 2 and 4, respectively.

Because the wave field at the interface of two adjacent layers satisfies the connection condition, we can therefore get the relationship of the field amplitudes A in different layers. There are two different kinds of interface in the $\Gamma X'$ direction: one is the interface of a uniform and a composite layer, such as the one between layer 1 and layer 2; the other is the interface of two composite layers, such as the one between layers 2 and 3. To simplify the theory we inset a uniform layer $2'$ between layers 2 and 3, and a uniform layer $3'$ between layers 3 and 4; but in the practical calculation we set the thickness of these two layers $2'$ and $3'$ to be zero. By this trick, only one kind of connection condition at the unform/composite interface needs to be considered. This condition can be written as

$$p^{(u)} = p^{(c)}, \quad x_0 < x < x_0 + \lambda, \tag{8}$$

and

$$v_y^{(u)} = \begin{cases} v_y^{(c)}, & x_0 < x < x_0 + \lambda \\ 0, & \text{else area in unit cell,} \end{cases} \tag{9}$$

where the superscripts (u) and (c) denote the variables in the uniform and composite layers, respectively.

Substituting Eqs. (1) and (5) into Eq. (8), and using the orthogonality of the waveguide modes, we get

$$\sum_{j=-M}^{+M} M_{mj}^{(u)}(A_j^{(u)+} + A_j^{(u)-}) = \sum_{n=0}^{N} M_{mn}^{(c)}(A_n^{(c)+} + A_n^{(c)-}), \quad m = 0,1,\ldots,N \tag{10}$$

with

$$M_{mj}^{(u)} = \int_{x_0}^{x_0+\lambda} \cos\frac{m\pi(x-x_0)}{\lambda} e^{i(K_x+G_j)x} dx, \tag{11}$$

$$M_{mn}^{(c)} = \int_{x_0}^{x_0+\lambda} \cos\frac{n\pi(x-x_0)}{\lambda} \cos\frac{m\pi(x-x_0)}{\lambda} dx = \begin{cases} 0, & m \neq n \\ \lambda/2, & m = n \neq 0 \\ \lambda, & m = n = 0, \end{cases} \tag{12}$$

where the superscripts (u) and (c) have the same meaning as in Eqs. (8) and (9).

Following the same way, we substitute Eqs. (2) and (6) into Eq. (9), and then get

$$\sum_{j=-M}^{+M} P_{mj}^{(u)}(A_j^{(u)+} - A_j^{(u)-}) = \sum_{n=0}^{N} P_{mn}^{(c)}(A_n^{(c)+} - A_n^{(c)-}), \quad m = 0, \pm 1, \ldots, \pm M \tag{13}$$

with

$$P_{mj}^{(u)} = \begin{cases} a\beta_j^{(u)}, & m = j \\ 0, & m \neq j \end{cases} \tag{14}$$

and

$$P_{mn}^{(c)} = \beta_n^{(c)} \int_{x_0}^{x_0+\lambda} e^{-i(K_x+G_m)x} \cos\frac{n\pi(x-x_0)}{\lambda} dx. \tag{15}$$

Here, the orthogonality of the Fourier components is used.

The matrices $M^{(u)}$, $M^{(c)}$, $P^{(u)}$, and $P^{(c)}$ are square matrices if we set $N+1 = 2M+1$. Suppose the propagating direction is from layer 1 to layer 4, then from Eqs. (10) and (13) we get a relation of the wave amplitudes between layer 1 and layer 2 as

$$\begin{pmatrix} A^{(2l)+} \\ A^{(1u)-} \end{pmatrix} = \begin{pmatrix} S_{11}^{12} & S_{12}^{12} \\ S_{21}^{12} & S_{22}^{12} \end{pmatrix} \begin{pmatrix} A^{(1u)+} \\ A^{(2l)-} \end{pmatrix}, \tag{16}$$

with the matrices

$$S_{11}^{12} = 2[(M^{(u)})^{-1}M^{(c)} + (P^{(u)})^{-1}P^{(c)}]^{-1}, \tag{17}$$

$$S_{12}^{12} = [(M^{(u)})^{-1}M^{(c)} + (P^{(u)})^{-1}P^{(c)}]^{-1}[(P^{(u)})^{-1}P^{(c)} - (M^{(u)})^{-1}M^{(c)}], \tag{18}$$

$$S_{21}^{12} = [(M^{(c)})^{-1}M^{(u)} + (P^{(c)})^{-1}P^{(u)}]^{-1}[(P^{(c)})^{-1}P^{(u)} - (M^{(c)})^{-1}M^{(u)}], \tag{19}$$

and

$$S_{22}^{12} = 2[(M^{(c)})^{-1}M^{(u)} + (P^{(c)})^{-1}P^{(u)}]^{-1}. \tag{20}$$

They are called scattering matrix [19,20], and the superscript "12" means from layer 1 to layer 2. $A^{(1u)}$ and $A^{(2l)}$ in Eq. (16) refer to the wave amplitudes at the upper boundary of layer 1 and the lower boundary of layer 2, respectively.

The relationship of the wave amplitudes between the lower and upper interfaces in a single layer (unform or composite) can also take the form of Eq. (16). For layer 1, we have

$$\begin{pmatrix} A^{(1u)+} \\ A^{(1l)-} \end{pmatrix} = \begin{pmatrix} S_{11}^{11} & S_{12}^{11} \\ S_{21}^{11} & S_{22}^{11} \end{pmatrix} \begin{pmatrix} A^{(1l)+} \\ A^{(1u)-} \end{pmatrix} \tag{21}$$

with

$$S_{12}^{11} = S_{21}^{11} = 0 \tag{22}$$

and

$$S_{11}^{11} = S_{22}^{11} = \begin{cases} e^{i\beta^{(u)}h} & \text{for diagonal terms} \\ 0 & \text{for nondiagonal terms,} \end{cases} \tag{23}$$

where the superscript of A has the same meaning as in Eq. (16), and h is the thickness of the layer, which equals zero

for the special case of the inserted layers $2'$ and $3'$.

In the same way, the scattering matrices $S_{ij}^{22'}$, $S_{ij}^{2'3}$, $S_{ij}^{33'}$, $S_{ij}^{3'4}$, and S_{ij}^{45} for each interface and the matrices S_{ij}^{22}, $S_{ij}^{2'2'}$, S_{ij}^{33}, $S_{ij}^{3'3'}$, and S_{ij}^{44} for each layer can be obtained, where i, j can take 1 or 2.

By a recursive deduction, we can eliminate the amplitudes of the inner layers [such as A^{1u} and A^{2l} in Eqs. (16) and (21)] and obtain the total scattering matrix that gives the relationship of the wave amplitudes at the lower boundary of layers 1 and 5 as

$$\begin{pmatrix} A^{(5l)+} \\ A^{(1l)-} \end{pmatrix} = \begin{pmatrix} S_{11} & S_{12} \\ S_{21} & S_{22} \end{pmatrix} \begin{pmatrix} A^{(1l)+} \\ A^{(5l)-} \end{pmatrix}. \tag{24}$$

On the other hand, for an infinite system, the periodicity along the y direction implies that

$$\begin{pmatrix} A^{(5l)+} \\ A^{(5l)-} \end{pmatrix} = e^{iK_y a} \begin{pmatrix} A^{(1l)+} \\ A^{(1l)-} \end{pmatrix}, \tag{25}$$

where K_y is the Bloch wave vector along the y direction. So a general eigenequation can be obtained by Eqs. (24) and (25) as

$$\begin{pmatrix} S_{11} & 0 \\ S_{21} & -I \end{pmatrix} \begin{pmatrix} A^{(1l)+} \\ A^{(1l)-} \end{pmatrix} = e^{iK_y a} \begin{pmatrix} I & -S_{12} \\ 0 & -S_{22} \end{pmatrix} \begin{pmatrix} A^{(1l)+} \\ A^{(1l)-} \end{pmatrix}, \tag{26}$$

where I is the unit matrix.

Notice that for different K_x and ω, Eq. (26) has many eigenvalues, but only those satisfying $e^{iK_y a}=1$ are the propagating Bloch waves in the system. For bands along the $\Gamma X'$, ΓM, and XM directions, the additional restricting condition with $K_x=0$, $K_x=K_y$, and $K_x=\pi/a$ must be satisfied, respectively. In principle, bands along the ΓX and $X'M$ directions can also be obtained by the conditions $K_y=0$ and $K_y=\pi/a$, respectively; but in practical calculation, only a few points can be obtained in these two directions. So we must get them in another way, which will be shown in the following section.

From Eq. (24), the reflection and transmission coefficients of a finite system with one period thickness along the y direction can also be calculated. If there is no negative propagating waves in layer 5, i.e., $A^{(5l)-}=0$, we have

$$A^{(5l)+} = S_{11} A^{(1l)+} \tag{27}$$

and

$$A^{(1l)-} = S_{21} A^{(1l)+}. \tag{28}$$

Obviously they are the transmission and reflection wave amplitudes corresponding to the incident wave amplitude $A^{(1l)+}$. In a similar way, the transmission and reflection coefficients of a finite system with multilayers can also be obtained.

More comprehension about the scattering matrix method for the general phononic or photonic crystals can be found in Refs. [19,20].

B. Along the ΓX direction

To calculate the band structure and transmission coefficient along the ΓX direction, we cut the unit cell along the X direction into two layers labeled as layers I and II in Fig. 1(b). The wave solutions in the composite layer II can take the same form as Eqs. (5)–(7) if we exchange x and y. From the figure, we can see that there are two kinds of waveguide modes in this layer. One is in the slit with $0<y<l$ and another is in the slit with $(a+l-t)/2<y<(a+l+t)/2$. The parameters in Eqs. (5)–(7) take different values in the two cases with $\lambda=l$ and $y_0=0$ in the former and $\lambda=t$ and $y_0=(a+l-t)/2$ in the latter. The connection condition at the interface between the uniform and composite layers should also be replaced by

$$p^{(u)} = p^{(c)}, \quad 0 < y < l, \text{ and } (a+l-t)/2 < y < (a+l+t)/2 \tag{29}$$

and

$$v_x^{(u)} = \begin{cases} v_x^{(c)}, & 0 < y < l \text{ and } (a+l-t)/2 < y < (a+l+t)/2 \\ 0, & \text{else range in unit cell.} \end{cases} \tag{30}$$

Following the same procedure of deducting Eq. (10), we get two equations from Eq. (29). In the region $0<y<l$, we have

$$\sum_{j=-M}^{+M} M_{mj}^{(u)} (A_j^{(u)+} + A_j^{(u)-}) = \sum_{n=0}^{N} M_{mn}^{(c)} (A_n^{(c)+} + A_n^{(c)-}), \quad m = 0,1,\ldots,N \tag{31}$$

with

$$M_{mj}^{(u)} = \int_0^l \cos\frac{m\pi y}{l} e^{i(K_y+G_j)y} dy, \tag{32}$$

$$M_{mn}^{(c)} = \int_0^l \cos\frac{n\pi y}{l} \cos\frac{m\pi y}{l} dy = \begin{cases} 0, & m \neq n \\ l/2, & m = n \neq 0 \\ l, & m = n = 0. \end{cases} \tag{33}$$

In the region $(a+l-t)/2<y<(a+l+t)/2$, we have

$$\sum_{j=-M}^{+M} Q_{mj}^{(u)} (A_j^{(u)+} + A_j^{(u)-}) = \sum_{n=0}^{N} Q_{mn}^{(c)} (B_n^{(c)+} + B_n^{(c)-}), \quad m = 0,1,\ldots,N \tag{34}$$

with

$$Q_{mj}^{(u)} = \int_{(a+l-t)/2}^{(a+l+t)/2} \cos\frac{m\pi[y-(a+l-t)/2]}{t} e^{i(K_y+G_j)y} dy, \tag{35}$$

$$Q_{mn}^{(c)} = \int_{(a+l-t)/2}^{(a+l+t)/2} \cos\frac{n\pi y}{t} \cos\frac{m\pi y}{t} dy = \begin{cases} 0, & m \neq n \\ t/2, & m = n \neq 0 \\ t, & m = n = 0, \end{cases} \tag{36}$$

where the variable B in Eq. (34) is the wave amplitude of the waveguide mode in the region $(a+l-t)/2<y<(a+l+t)/2$.

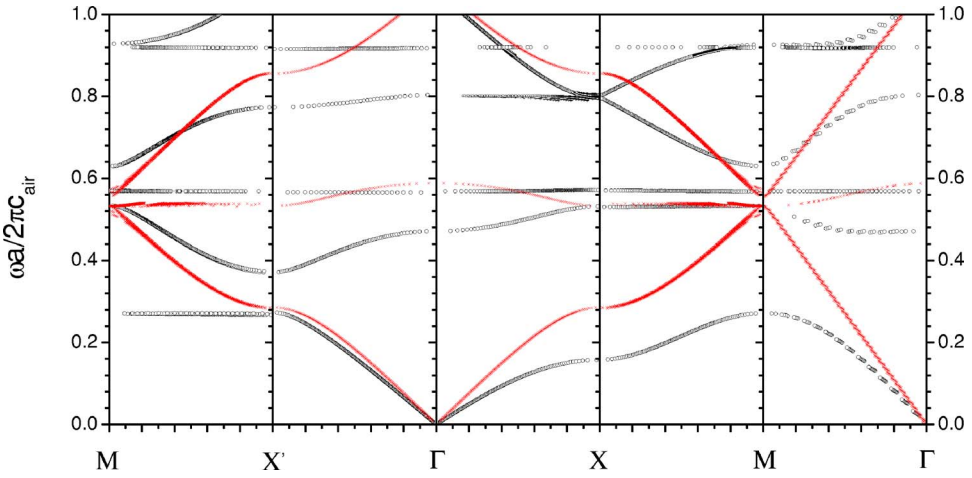

FIG. 2. (Color online) Band structure (empty circles) of the system shown in Fig. 1 with $l=0.2a$, $w=0.9a$, and $t=0.7a$ along the M-X'-Γ-X-M-Γ direction. Crosses display the results of the system without the resonant cavity (with $w=l=0.2a$ or $t=0$).

From Eq. (30), we have

$$\sum_{j=-M}^{+M} P_{mj}^{(u)}(A_j^{(u)+} - A_j^{(u)-}) = \sum_{n=0}^{N} P_{mn}^{(c)}(A_n^{(c)+} - A_n^{(c)-}) + \sum_{n=0}^{N} R_{mn}(B_n^{(c)+} - B_n^{(c)-}), \quad m = 0, \pm 1, \ldots, \pm M \tag{37}$$

with

$$P_{mj}^{(u)} = \begin{cases} a\beta_j^{(u)}, & m = j \\ 0, & m \neq j, \end{cases} \tag{38}$$

$$P_{mn}^{(c)} = \beta_n^{cl} \int_0^l e^{-i(K_y+G_m)y} \cos\frac{n\pi y}{l} dy, \tag{39}$$

and

$$R_{mn} = \beta_n^{ct} \int_{(a+l-t)/2}^{(a+l+t)/2} e^{-i(K_y+G_m)[y-(a+l-t)/2]} \cos\frac{n\pi y}{t} dy, \tag{40}$$

where β_n^{cl} and β_n^{ct} are the wave vectors along the x direction in the regions $0<y<l$ and $(a+l-t)/2<y<(a+l+t)/2$ in layer II, respectively.

Equations (31), (34), and (37) give the relationship among $A^{(u)}$, $A^{(c)}$, and $B^{(c)}$ at the interface of layers I and II, which cannot be used directly in the scattering matrix method. The variables $B^{(c)}$ in Eqs. (34) and (37) must be eliminated first.

We notice that the variables $B^{(c)+}$ and $B^{(c)-}$ satisfy the equation

$$B_n^{(c)-} = e^{i\beta_n^{ct}(w-l)} B_n^{(c)+}. \tag{41}$$

Using Eq. (34), it is easy to rewrite Eq. (37) as

$$(P^{(u)} - H)A^{(u)+} - (P^{(u)} + H)A^{(u)-} = P^{(c)}(A^{(c)+} - A^{(c)-}) \tag{42}$$

with

$$H = R(I - e^{i\beta^{ct}(w-L)})[Q^{(c)}(I + e^{i\beta^{ct}(w-l)})]^{-1} Q^{(u)}. \tag{43}$$

Now, Eqs. (31) and (42) look more like Eqs. (10) and (13). Following the same procedure of Eqs. (16)–(25) an eigenequation like Eq. (26) can be obtained. In the numerical calculation along the ΓX direction, we should first set the values of K_y and ω. We pick out the eigenvalues satisfying $e^{ik_x a}=1$ and then get the band structure along ΓX and $X'M$ by the conditions $K_y=0$ and $K_y=\pi/a$, respectively. The transmission coefficient along this direction can also be calculated in the same way as Eqs. (27) and (28) if the total scattering matrix is obtained.

III. RESULTS AND DISCUSSION

A typical band structure of the SC with $w=0.9a$, $t=0.7a$, and $l=0.2a$ is shown in Fig. 2 (by empty circles). The corresponding band structure of the conventional system without resonant cavity ($w=l=0.2a$ or $t=0$) is also shown (by crosses) in the same figure. From the figure we can see that, compared with the band structure of the conventional system, the degeneracy of the lowest three bands at the M point is broken and an ABG appears. It is well-known that the mechanism of the ABG in conventional PCs is usually based on the Bragg scattering, and the position of such an ABG, if it exists, often appears at an angular frequency ω of the order of c/a [17]; but in the present model, another kind of ABG appears at the frequency well below the Bragg limit due to the interaction of the resonant modes in the cavities. The width and position of this ABG depend strongly on the resonant frequency, quality factor of the mode, and the distance between the nearest cavities, which provides a convenient way to adjust the band structure by changing the characters of the cavity modes. Therefore we conclude that the ABG in Fig. 2 is a band gap of resonant type and it is expected that the band structure can be modified by changing the shape of the open cavity. We also notice that the coupling of the high order resonant modes in the cavity leads to some absolute flat bands (dispersiveness bands) in the spectrum [17], such as those that appear around $\omega a/2\pi c_{air}=0.57$ and 0.92 in Fig. 2.

To see the relationship between the band structure and the shape of the resonant cavity, we plot the lowest ABG as a function of t and w in Figs. 3(a) and 3(b), respectively. From Fig. 3(a) we can see that both the width of the ABG and the band edge change when t decreases from $0.7a$ to $0.25a$ for fixed $l=0.2a$ and $w=0.9a$. The ABG has the largest value at $t=0.7a$, then becomes smaller when t decreases, and finally

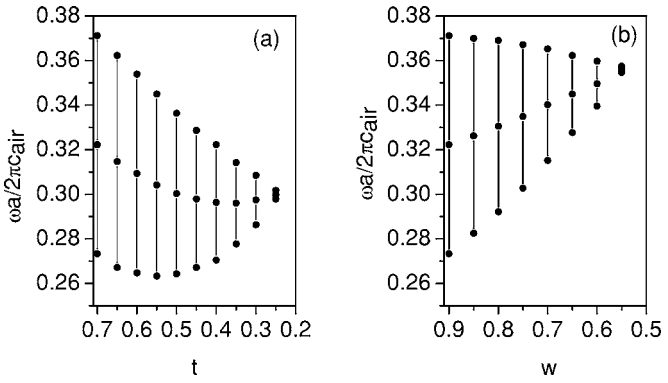

FIG. 3. The band gaps of the system with (a) $w=0.9a$, $l=0.2a$ for different t, and (b) $t=0.7a$, $l=0.2a$ for different w. The full circles denote the lower, upper band edges and the middle frequency of the gaps.

closes at $t=0.25a$. The upper band edge changes almost linearly as t decreases, but the lower band edge first decreases and then increases when t changes from $0.7a$ to $0.25a$, with the minimum appearing around $t=0.55a$. In Fig. 3(b), $l=0.2a$ and $t=0.7a$ are fixed and w is a variable. It is observed that the largest ABG also appears around $w=0.9a$. The upper band edge decreases slowly when w drops from $0.9a$ to $0.55a$, but the lower band edge increases almost linearly. Figure 3 shows that the systems with different t and/or w have quite different band structures. In the case of Fig. 3(a), the change of t not only influences the frequency and quality factor of the resonant cavity, but also influences the distance between the nearest cavities (and then the coupling strength of cavity modes). In the case of Fig. 3(b), only the resonant frequency and quality factor are modified when w changes. We know that both the width of the ABG and its position in frequency are important in a sound proof material, so an audible sound proof may be made of a SC with a resonant cavity.

Because the ABG appears in Fig. 2, the lowest band of the SC with a resonant cavity is flatter than that of conventional SCs. As is argued in Ref. [18], the PC structure can be treated as an effective medium if the wavelength of the propagating wave is below its diffraction limit, and an effective sound velocity v_{eff} can be defined directly by ω/k (the slope of the band line). So the flattening of the lowest band suggests that a smaller effective velocity v_{eff} can be obtained in the present model than that in conventional PCs, which indicates that a material for a sound lens with a large refractive index (defined as $n=c_{air}/c_{eff}$) can be realized [14]. Obviously, the effective velocity v_{eff} can be modified by the shape of the resonant cavity, and a descending (ascending) lower band edge of the ABG corresponds to a decreasing (increasing) slope of the lowest band line. From Fig. 3, we can expect that the largest n will appear in the system with $t=0.55a$, $l=0.2a$, and $w=0.9a$.

We have pointed out in Sec. II that the present method can also be used to study the transmission properties efficiently. To show this, the transmission coefficient (energy flow) of a finite sized system with $t=0.7a$, $l=0.2a$, and $w=0.9a$ is investigated. We calculate the transmission coefficients through surfaces normal to the ΓX and $\Gamma X'$ directions with

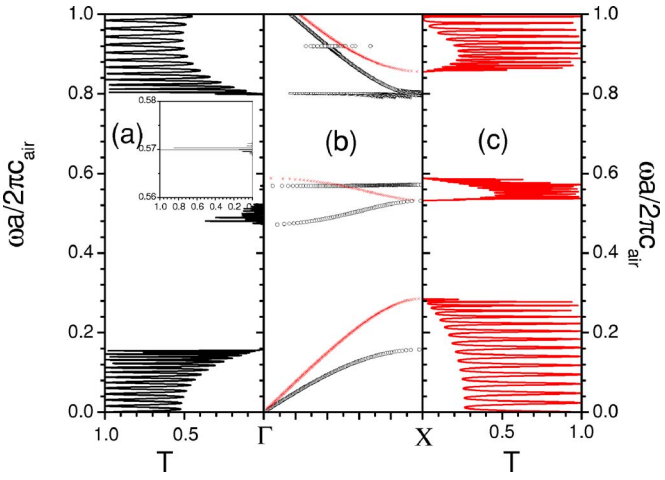

FIG. 4. (Color online) The transmission coefficient along the ΓX direction of the system discussed in Fig. 2. (a) and (c) correspond to the systems with and without a resonant cavity, respectively. The inset of (a) is the enlargement around $\omega a/2\pi c_{air}=0.6$. (b) is the band structure, in which empty circles and crosses show the bands of the system with and without resonant cavity, respectively.

thickness of layers being 16 periods, respectively. The results are shown in Figs. 4 and 5, in which the result for systems with and without resonant cavities are shown in (a) and (c), respectively. We can see that the band structures coincide with the transmission spectra [shown in (b) of the same figures] very well except the absolute flat bands. The inset of Fig. 4(a) [Fig. 5(a)] shows that the flat band around $\omega a/2\pi c_{air}=0.57$ (0.92) can be excited by an external incident wave. So the absence of the peak in Fig. 5(a) may be caused by the numerical error—a sharp peak is usually difficult to display in the numerical calculation. Figures 4 and 5 also show another interesting phenomena: in the low frequency region, the transmission coefficient of the SC with resonant cavity is higher than that of the conventional system. This is caused by the structure itself: the cavity helps the long wavelength wave pass though the system. We discussed in Ref. [18] that the local minimum of the transmis-

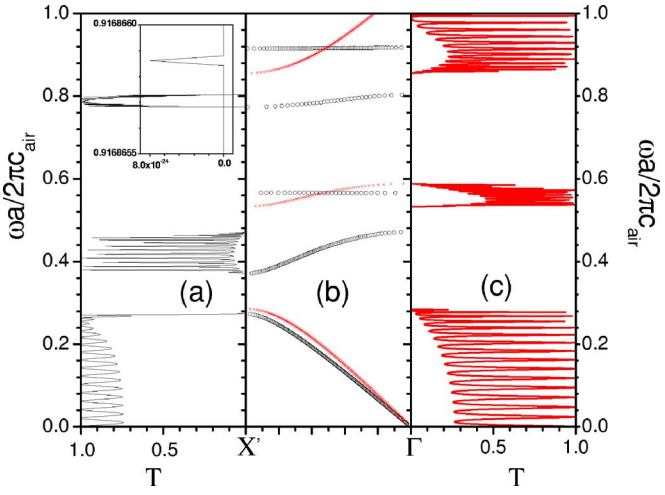

FIG. 5. (Color online) Same as Fig. 4 but along the $\Gamma X'$ direction. The inset of (a) is the enlargement around $\omega a/2\pi c_{air}=0.91$.

sion coefficient is determined by the difference of the acoustic impedance (or effective impedance) between air (Z_{air}) and SC (Z_{SC}), which will be close to 1 when Z_{air}/Z_{SC} tends to be unity. Here, we see from Figs. 4 and 5 that in the long-wavelength region, Z_{SC} in the resonant cavity system is closer to Z_{air} than that of conventional SCs; but Z_{SC} takes different values in the ΓX and $\Gamma X'$ directions, which means the studied system is anisotropic.

IV. BRIEF SUMMARY

We present a successful method to deal with the two-dimensional SC which is constructed by periodically arranging rectangular rods with an open resonant cavity in air. Both the band structure and the transmission properties are calculated efficiently. A relationship between the band structure and the shape of the open resonant cavity is given. The numerical results show that the width of the ABG and the effective acoustic velocity in the long wavelength region are determined by the shape of the cavity. From the transmission spectra, we find that the existence of the resonant cavity can also enhance the transmission ratio, which means that Z_{air}/Z_{SC} tends to be unity in the long wavelength region.

ACKNOWLEDGMENT

This work was supported by the National Natural Science Foundation of China under Grants No. 10474021 and No. 50573023.

[1] D. Caballero, J. Sanchez-Dehesa, C. Rubio, R. Martinez-Sala, J. V. Sanchez-Perez, F. Meseguer, and J. Llinares, Phys. Rev. E **60**, R6316 (1999).
[2] Manvir S. Kushwaha, Appl. Phys. Lett. **70**, 3218 (1997).
[3] J. O. Vasseur, P. A. Deymier, A. Khelif, Ph. Lambin, B. Djafari-Rouhani, A. Akjouj, L. Dobrzynski, N. Fettouhi, and J. Zemmouri, Phys. Rev. E **65**, 056608 (2002).
[4] Yun Lai, Xiangdong Zhang, and Zhao-Qing Zhang, J. Appl. Phys. **91**, 6191 (2002).
[5] C. Goffaux, F. Maseri, J. O. Vasseur, B. Djafari-Rouhani, and Ph. Lambin, Appl. Phys. Lett. **83**, 281 (2003).
[6] J. V. Sanchez-Perez, D. Caballero, R. Martinez-Sala, C. Rubio, J. Sanchez-Dehesa, F. Meseguer, J. Llinares, and F. Galvez, Phys. Rev. Lett. **80**, 5325 (1998).
[7] F. Cervera, L. Sanchis, J. V. Sanchez-Perez, R. Martinez-Sala, C. Rubio, F. Meseguer, C. Lopez, D. Caballero, and J. Sanchez-Dehesa, Phys. Rev. Lett. **88**, 23902 (2002).
[8] Liang Feng, Xiao-Ping Liu, Ming-Hui Lu, Yan-Bin Chen, Yan-Feng Chen, Yi-Wei Mao, Jian Zi, Yong-Yuan Zhu, Shi-Ning Zhu, and Nai-Ben Ming, Phys. Rev. Lett. **96**, 14301 (2006).
[9] L. Sanchis, A. Hakansson, F. Cervera, and J. Sanchez-Dehesa, Phys. Rev. B **67**, 035422 (2003).
[10] D. Torrent, A. Hakansson, F. Cervera, and J. Sanchez-Dehesa, Phys. Rev. Lett. **96**, 204302 (2006).
[11] B. C. Gupta and Zhen Ye, Phys. Rev. E **67**, 036603 (2003).
[12] L. Sanchis, F. Cervera, J. Sanchez-Dehesa, J. V. Sanchez-Perez, C. Rubio, and R. Martinez-Sala, J. Acoust. Soc. Am. **109**, 2598 (2001).
[13] Y. Tanaka, Y. Tomoyasu, and S.-I. Tamura, Phys. Rev. B **62**, 7387 (2000).
[14] Xinhua Hu, C. T. Chan, and Jian Zi, Phys. Rev. E **71**, 055601(R) (2005).
[15] Zhilin Hou, Xiujun Fu, and Youyan Liu, Phys. Rev. B **73**, 024304 (2006).
[16] Zhilin Hou, Xiujun Fu, and Youyan Liu, Phys. Rev. B **70**, 014304 (2004).
[17] R. Sainidou, B. Djafari-Rouhani, Y. Pennec, and J. O. Vasseur, Phys. Rev. B **73**, 024302 (2006).
[18] Zhilin Hou, Fugen Wu, Xiujun Fu, and Youyan Liu, Phys. Rev. E **71**, 037604 (2005).
[19] Yuanwei Yao, Zhilin Hou, Yongjun Cao, and Youyan Liu, Physica B **388**, 75 (2007).
[20] Zhi-Yuan Li and Lan-Lan Lin, Phys. Rev. E **67**, 046607 (2003).